Biochimica et Biophysica Acta 1861 (2017) 839–847

Contents lists available at ScienceDirect

Biochimica et Biophysica Acta

journal homepage: www.elsevier.com/locate/bbagen

Synergistic effect of electric field and lipid oxidation on the permeability of cell membranes

M. Yusupov *, J. Van der Paal, E.C. Neyts, A. Bogaerts

Research Group PLASMANT, Department of Chemistry, University of Antwerp, Universiteitsplein 1, B-2610 Antwerp, Belgium

ARTICLE INFO

Article history:
Received 9 November 2016
Received in revised form 25 December 2016
Accepted 26 January 2017
Available online 27 January 2017

Keywords:
Cell membrane
Molecular dynamics simulation
Reactive oxygen species
Electric field
Plasma medicine
Electroporation

ABSTRACT

Background: Strong electric fields are known to affect cell membrane permeability, which can be applied for therapeutic purposes, e.g., in cancer therapy. A synergistic enhancement of this effect may be accomplished by the presence of reactive oxygen species (ROS), as generated in cold atmospheric plasmas. Little is known about the synergy between lipid oxidation by ROS and the electric field, nor on how this affects the cell membrane permeability.

Method: We here conduct molecular dynamics simulations to elucidate the dynamics of the permeation process under the influence of combined lipid oxidation and electroporation. A phospholipid bilayer (PLB), consisting of di-oleoyl-phosphatidylcholine molecules covered with water layers, is used as a model system for the plasma membrane.

Results and conclusions: We show how oxidation of the lipids in the PLB leads to an increase of the permeability of the bilayer to ROS, although the permeation free energy barriers still remain relatively high. More importantly, oxidation of the lipids results in a drop of the electric field threshold needed for pore formation (i.e., electroporation) in the PLB. The created pores in the membrane facilitate the penetration of reactive plasma species deep into the cell interior, eventually causing oxidative damage.

General significance: This study is of particular interest for plasma medicine, as plasma generates both ROS and electric fields, but it is also of more general interest for applications where strong electric fields and ROS both come into play.

1. Introduction

Over the past decade, cold atmospheric plasma (CAP), i.e., an ionized gas near room temperature, has shown promising applications in cancer therapy [1–4]. There is a growing body of literature to support the claim that CAP may selectively target the destruction of cancer cells [4–6], which might give an advantage to CAP over traditional anti-cancer methods, such as chemotherapy and radiotherapy.

The possible selectivity of CAP towards cancer cells is most probably due to the noticeable rise of intracellular reactive oxygen species (ROS) occurring in cancer cells compared to normal cells upon the same CAP treatment [7–11]. However, the underlying mechanisms explaining the enhanced concentration of ROS in cancer cells still remain elusive.

Several studies in literature have tried to understand these mechanisms of plasma-based cancer treatment [6,12,13]. Yan et al. proposed a mechanism for the possible selectivity of ROS towards cancer cells, based on aquaporins (AQPs), i.e., the only verified H_2O_2 channels on the cytoplasmic membrane of cancer cells [6]. H_2O_2 is regarded as one of the main anti-cancer ROS from CAP based on in vitro studies [6]. They found that after the CAP treatment, CAP-generated H_2O_2 species diffuse into cancer cells significantly faster than in homologous normal cells, causing a significantly higher rise of ROS in cancer cells compared to normal cells [6]. Recently, Szili et al. investigated how plasma and plasma-generated ROS might interact with real cells in contrast to synthetic phospholipid (PL) vesicles [12]. The authors suggested some mechanisms for the transport of reactive plasma species into cells, i.e., by interplay of concentration gradients of short and long lived ROS combined with other effects, including electric field [12]. Van der Paal et al. found that cholesterol can protect oxidized membranes against pore formation [13,78]. This result is of great interest for plasma-based cancer therapy, as cancer cells typically contain less cholesterol in their plasma membrane, so the above observation can also explain the possible selectivity of plasma treatment towards cancer cells, as they allow the reactive plasma species to reach the cell interior more easily through pore formation.

It is known that the plasma generated reactive species first interact with the cell membrane, chemically modifying (e.g., oxidizing) its lipids, and it is important to elucidate the penetration abilities of the reactive species through the oxidized lipid bilayer, which is exactly the first subject of the present paper. This allows us to find out whether there is a need for specific protein channels like AQPs, or whether the formation

* Corresponding author.
E-mail address: maksudbek.yusupov@uantwerpen.be (M. Yusupov).

http://dx.doi.org/10.1016/j.bbagen.2017.01.030
0304-4165/

of pores is necessary in order to deliver reactive plasma species into the cell interior to cause oxidative stress.

In the context of plasma medicine, several experimental investigations have been performed on PL vesicles as simple models for cell membranes, to study the oxidation of lipids, their structural and chemical modifications, as well as the transport of ROS across the PL membranes [12,14–18]. For example, Hammer et al. showed that a three minute CAP treatment of liposomes leads to an increase in the fluidity of the PL bilayer (PLB) [14]. Maheux et al. reported a more negative zeta potential after CAP treatment of small unilamellar vesicles [15]. The authors indicated that a larger number of chemical modifications takes place on the PLs, leading to a more negatively charged surface of the treated liposomes [15]. Further, Hong et al. showed that CAP treatment of PL vesicles can lead to an ingress of ROS into the vesicles without damaging the cell membrane integrity [16]. They also observed a significant reduction of the transfer efficiency of ROS into the vesicles in the presence of serum [16]. The permeation of OH radicals and their reaction with intramembrane molecules were observed in [17] using giant unilamellar vesicles. Furthermore, Tero et al. observed the formation of pores (with sizes of 10 nm–1 μm) induced by CAP on artificial planar lipid bilayers formed at solid-liquid interfaces [18]. Thus, to summarize, CAP treatment of the cell membrane leads to oxidation of the lipids, which subsequently affects the bilayer fluidity and lipid disorder, thereby altering the permeability of the membrane to reactive plasma species.

Similar conclusions were made in numerical studies applying molecular dynamics (MD) simulations on oxidized PLBs [13,19–21]. In general, the simulations reveal an overall increase in the membrane permeability [19], a change in the lipid mobility in the PLB [20], pore creation and bilayer disintegration [21] upon introduction of oxidized lipids.

It is important to realize that in addition to the creation of reactive species, some CAP sources also generate strong electric fields, ranging from a few up to 100 kV/cm (see e.g., [22–30]). These electric fields may play an important and synergistic role in plasma-cell interactions [30], as they are high enough to induce pore formation in membranes [31]. Thus, in order to gain insight in the plasma-cell interactions, the effect of electric fields should be taken into account together with the effect of reactive plasma species. Therefore, the second subject of the current paper will be the study of the effect of electric field.

The application of high electric fields can indeed disturb the integrity of the membrane, through the creation of pores either temporarily or permanently, which leads to cell membrane permeabilization. This method is known as electroporation and nowadays is employed in different fields, including medicine [32–34]. Electroporation is widely used for the delivery of chemical species, such as ions and small molecules, dyes, drugs or genetic materials into cells [33,35,36] and it is successfully applied for cancer treatment [37,38]. Thorough discussions on electroporation and its applications are given in excellent reviews [31,35, 37–42]. There are also MD studies devoted to electroporation, where various investigations are conducted using PLB model systems, e.g., the study of the mechanisms of membrane electroporation [43–45], the effect of cholesterol on the electroporation threshold [46], transport of siRNA through lipid membranes [47], the phosphatidylserine translocation [48] as well as calcium-induced adsorption of DNA on a lipid membrane [49]. More information about MD studies on electroporation can be found in [50–52]. Although much research has been performed in the field of electroporation, still little is known about the synergy between ROS and the electric field, and more specifically on how this affects the cell membrane permeability.

Thus, based on the above mentioned considerations, in this paper we investigate the combined effect of the electric field together with lipid oxidation, as both effects are important in plasma-cell interactions, and thus the combination of both is highly relevant for studying the effect of plasma on living cells. To our knowledge, this combined effect has not yet been investigated before in the context of plasma medicine. Besides the direct interest for plasma medicine, this study is also of broader interest for other applications where both strong electric fields and ROS come into play. Note that the results presented in this study are not limited to cancer therapies. They are also highly relevant to a wider range of applications of plasma in medicine, such as treatment of skin diseases, wound healing, etc. (see e.g., [53,54] in which the effect of the electric field as well as the delivery of reactive plasma species into a tissue model are discussed).

2. Simulation setup

In this study we carry out MD simulations to study the electroporation process together with the effect of oxidation of the PLs. Specifically, we investigate two cases. Firstly, we study the translocation of ROS (more specifically OH, HO_2, H_2O_2 and O_2) through native and oxidized PLBs, calculating their permeation free energy profiles, to elucidate the penetration capabilities in the absence of an electric field. Secondly, we investigate the effect of the electric field on pore formation again in native and oxidized bilayers. Note that other ROS and reactive nitrogen species (e.g., O_3, NO_2, $ONOO^-$) are also important and they are generally believed to also play a key role in plasma treatment [4,55]. However, no accurate force field parameter sets for these species are currently available, and therefore the behavior of these species cannot yet be investigated.

As a model system we use the PLB shown in Fig. 1, representing the cell membrane. It is composed of 128 lipids surrounded by two water leaflets, each of which contains 4000 water molecules (i.e., in total 8000 water molecules), corresponding to a hydration level of ~63 waters/lipid. The PL investigated is 1,2-dioleoyl-*sn*-glycero-3-phosphocholine

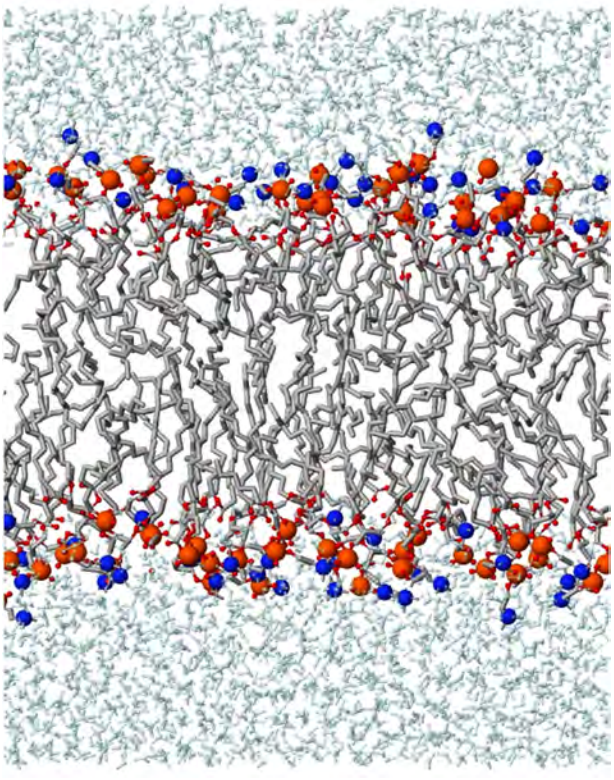

Fig. 1. Native DOPC PLB to be treated with MD simulations. The PLB consists of 128 DOPC molecules with 8000 water molecules organized in two lamellae (i.e., 64 DOPCs, with corresponding water layer, at the top and 64 at the bottom). The water layers, oxygen atoms and lipid tails are shown in cyan, red and gray colors, respectively. The P (orange) and N (blue) atoms are depicted with bigger beads, for the sake of clarity. The color legend also applies to the other similar figures below.

(DOPC), which is illustrated in Fig. 2. To study the effect of oxidized PLs, two oxidation products of DOPC are included in the simulated systems, i.e., a peroxide and an aldehyde (see also Fig. 2). The peroxide and aldehyde were chosen because it is shown that these are two of the major oxidation products [56]. The peroxide is the end product of the main lipid peroxidation reaction, whereas the aldehyde product is formed due to a ring closing and opening reaction of the intermediate lipid peroxide radical, which yields two aldehydes. To create multiple oxidized membranes, 10, 20, 30, 40 or 50 mol% of the DOPC molecules in the native PLB structure are replaced by one of both oxidized PLs. The Packmol package is used to create the different structures [57].

Once the initial configurations of the membranes are generated, an energy minimization is performed using the steepest descent algorithm. Afterwards, the systems are equilibrated during 110 ns, of which the last 10 ns are used for further analysis. During all runs, the GROMOS43A1-S3 force field is applied [58]. Note that this force field is an all-atom force field except for the methyl and methylene groups that are treated as united atoms. The parameters for peroxide and aldehyde groups in the oxidized PLs (see Fig. 2) are obtained from [19]. The ROS investigated in this study are, however, not present in this force field, so the relevant parameters are taken from literature [59]. The simulations are performed in the NPT-ensemble by applying the Nose-Hoover thermostat [60] and the semi-isotropic Parinello-Rahman barostat [61] (i.e. pressure coupling is isotropic in x and y direction, but different in z direction, which ensures that $L_x = L_y$). The applied reference temperature is 310 K combined with a coupling constant of 0.2 ps, whereas the applied reference pressure is 1 atm combined with a compressibility of 4.5×10^{-5} bar^{-1} and a coupling constant of 1 ps. Periodic boundary conditions are applied in all Cartesian directions. Considering the non-bonded interactions, a 1.0 nm cut-off is applied for the van der Waals interactions. The electrostatic interactions, on the other hand, are calculated using the PME-method [62,63], using a 1.0 nm cut-off for the real-space interactions in combination with a 0.15 nm spaced-grid for the reciprocal-space interactions and a fourth-order B-spline interpolation. All simulations and analyses mentioned in this study are performed using the GROMACS 5.1 package [63].

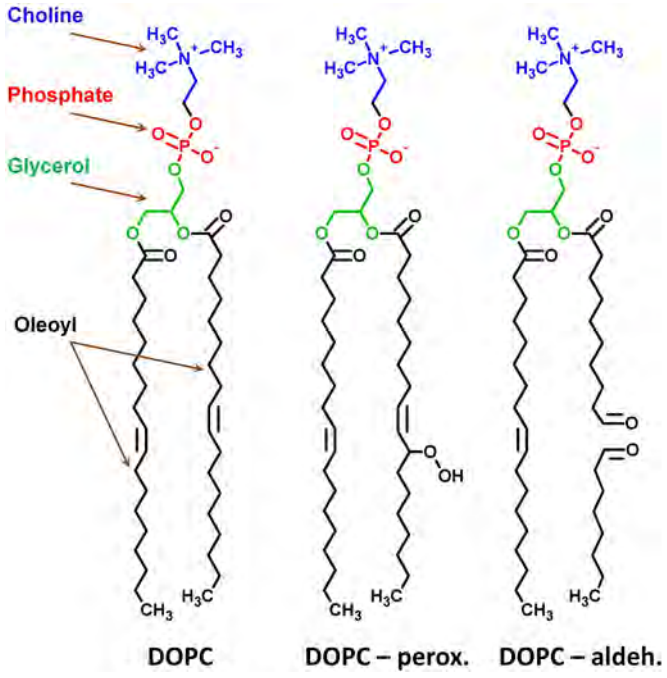

Fig. 2. Schematic illustrations of the native (DOPC) and oxidized (DOPC-perox. and DOPC-aldeh.) PLs.

2.1. Free energy profiling

To understand the effect of lipid oxidation on the permeation of ROS, umbrella sampling (US) simulations are performed for H_2O_2 and O_2 molecules as well as for HO_2 and OH radicals, in native and 50% oxidized structures (both aldehyde and peroxide). Initial structures for these simulations are selected as random frames from the last ns of the corresponding equilibration simulation (see above). For each energy profile, 150 US windows are defined along the bilayer normal (z-axis), which are separated by 0.5 Å. In this manner, the sampling windows span the entire membrane system. Five US windows, separated by 15 Å, are sampled during each simulation to save computational resources. A harmonic bias with a force constant of 1000 $kJ \cdot mol^{-1} \cdot nm^{-2}$ is applied along the z-direction on the reactive species, to restrict their motion. After an extra equilibration of 3 ns, a 2 ns simulation is performed during which the US histograms are collected. The conditions used in these simulations are identical to those used during the equilibration runs (see above). Free energy profiles are constructed by using a periodic version of the weighted histogram analysis method (WHAM) [64], as is implemented in the *g_wham* tool of GROMACS. The final energy profiles are obtained by averaging over four US simulations, which differ from one another based on their starting structure, to allow for some statistical variations. The energy barriers and their associated standard deviations (see Table 1 below) are obtained by calculating the difference between energy minimum and maximum in each energy profile and averaging them over four US simulations. Note that the US simulations need a lot of computational resources and are therefore computationally expensive. In total 1440 US simulations are performed for the calculation of the free energy profiles.

2.2. Electric field simulations

To investigate the effect of the electric field on the different membrane structures, additional simulations are performed using the last frame of each equilibrated structure as input, and applying an electric field of varying strength. In case of the oxidized structures, electric field strengths of 300, 400 and 500 mV/nm are investigated, whereas in the case of the native membrane, electric field strengths of 400, 450, 500, 550 and 600 mV/nm are used. Note that these are typical electric field values used in electroporation simulations (see e.g., [44–46,48,65,66]). However, the values are much higher than the electric fields applied in electroporation experiments [31] or in plasma medicine applications [22–30]. Experimentally, applied field strengths might vary between 0.1 and 100 kV/cm (i.e., between 0.01 and 10 mV/nm), which are at least an order of magnitude lower than the fields used in MD simulations. In fact, the macroscopic field applied to the system in experiments is not equivalent, by any means, to the field which is felt by the membrane (and which is applied in MD simulations), and therefore these values should not be directly compared. Specifically, the macroscopic electric field used in experiments is only the spatially averaged electric field obtained from the applied voltage between electrodes, whereas the microscopic electric field across the membrane should be determined from the transmembrane potential. The latter is not straightforward to determine from the global value. Therefore, a constant electric field is used in MD simulations to study the electroporation process. The transmembrane potential difference, in this case, is simply determined from a multiplication of this electric field to the size of the simulation box in the field direction (mostly z axis). The time dependent microscopic transmembrane potential was determined from the global value (i.e., the macroscopic electric field) in [67,68] using a so-called distributed circuit model. The determined maximum value of the transmembrane potential (i.e., >2 V, when the external applied electric field is 10 mV/nm [67,68]) corresponds fairly well to the values of the transmembrane voltage needed for pore formation in MD simulations (see e.g., [45,48,69] as well as below). Thus, despite the fact that the temporal behavior is excluded, the applied constant

electric fields in MD studies can give valuable information about the electroporation process on the atomic scale. Moreover, these microscopic electric fields can be correlated with the macroscopic electric fields through the transmembrane potential and the direct proportionality can be obtained between them.

The simulations are run for 20 ns, using the same simulation parameters as in the equilibration runs. By selecting 10 frames from the last 10 ns of the equilibration run (i.e., one frame every ns), 10 independent electric field simulations are performed. For each simulation, the time until the occurrence of pore formation is calculated, which is then averaged over all independent simulations.

2.3. Analysis

To analyze the various properties of the simulated membranes, the last 10 ns of each equilibration run is used. The bilayer thickness is defined as the average distance along the z-axis between the center of mass of the phosphorus atoms of both leaflets, using the *gmx_distance* command of GROMACS. The area per lipid is calculated from the average box size in the xy-plane, divided by the number of lipids in one leaflet, i.e., $L_x \times L_y/64$. This value gives thus an average area over both native and oxidized PLs. The average box size in the xy-plane, as well as the average box size in the z-direction are calculated using the *gmx_energy* command. The error bars shown in the results below are all calculated using the block method of Hess [70].

3. Results and discussion

As mentioned above, this study is composed of two parts. We first study the translocation of ROS (namely, OH, HO_2, H_2O_2 and O_2) through native and oxidized PLBs. This gives us information about the penetration abilities of ROS through these bilayers, when there is no pore formed in the PLBs. Indeed, the effect of the electric field is excluded here, and the oxidation degree is up to 50%, which is high enough to observe the effect of oxidation, but low enough so that pore formation does not yet occur [13]. This allows us to elucidate whether or not the formation of pores is necessary in order to deliver ROS (and other molecules) into the cell interior. Subsequently, we investigate the effect of the electric field on pore formation, again in native and oxidized bilayers. This allows us to determine how the electric field facilitates pore formation, when oxidation takes place in the PLBs. Thus, in this study two research questions will be investigated, i.e., (i) can ROS penetrate through a native or oxidized PLB in the absence of an electric field, and if not, (ii) which electric field strengths are needed to create pores in both native and oxidized PLB?

3.1. Translocation of ROS through native and oxidized PLBs

Fig. 3 illustrates the free energy profiles of ROS across native and 50% oxidized PLBs, for both the peroxide and aldehyde oxidation products. We chose the 50% oxidized systems, but we expect that other oxidation degrees will give similar results, albeit less pronounced. Moreover, these calculations of the energy profiles are computationally expensive (see Section 2.1).

As is clear from Fig. 3, in all three cases hydrophobic O_2 molecules can easily travel towards the lipid tails without significant energy barriers for permeation. As soon as they reach the apolar center of the bilayer, they remain stable there, as their activation free energies from the center to the water layer are still relatively high (see Table 1). The H_2O_2 molecules have a free energy minimum near the head group region, i.e., they prefer to stay close to the phosphate groups (see red dashed line in Fig. 3). This is due to the favorable H-bond interactions with phosphate groups [59]. The HO_2 and OH radicals can stay deeper in the PLB. This is more pronounced for HO_2 with significantly deeper free energy minima, i.e., −16.5, −15.0 and −15.6 kJ/mol, in the case of the native, 50% peroxidized and 50% aldehyde oxidized PLBs,

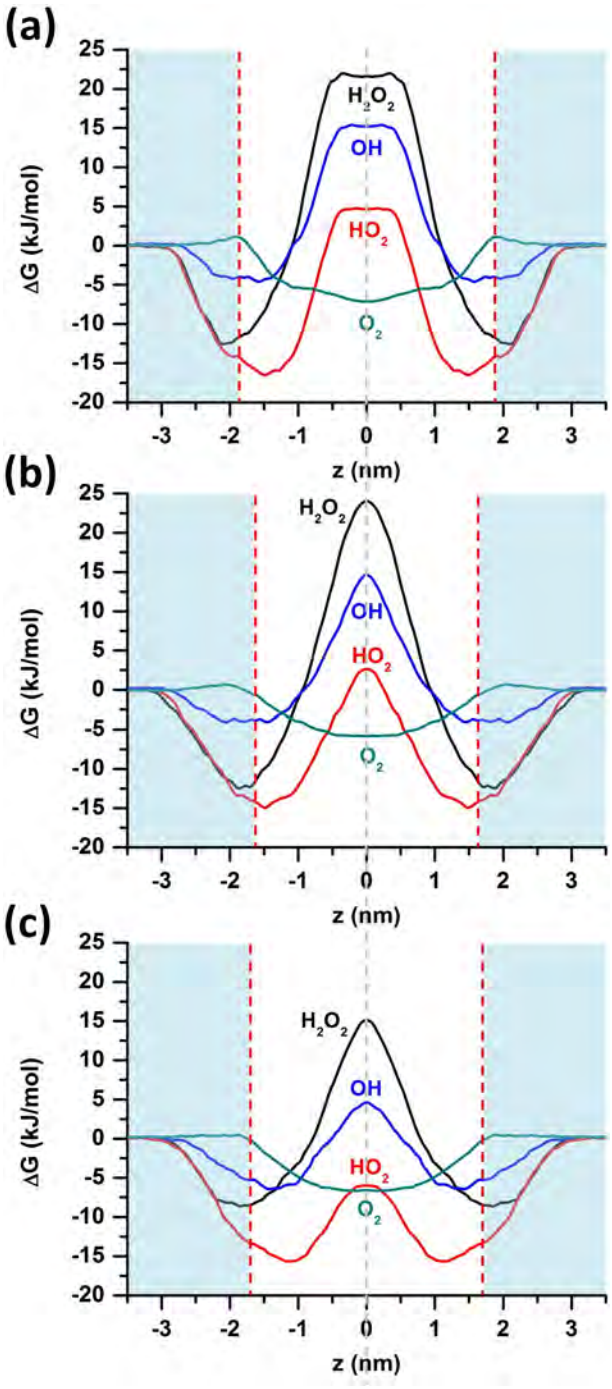

Fig. 3. Free energy profiles for the translocation of ROS across native (a), 50 mol% peroxidized (b) and 50 mol% aldehyde oxidized (c) PLBs. The red dashed lines indicate the average positions of the phosphate groups (i.e., average bilayer thickness, cf. Table 2). The gray dashed line corresponds to the bilayer center. The water layers are highlighted by the light blue shaded color.

respectively (see Fig. 3). The behavior of these species can again be explained from the H-bonds they form [59]. HO_2 radicals are better proton donors but weaker proton acceptors than water [59,71] and they more likely interact with ester groups found between the head groups and the lipid tails [59]. OH radicals, on the other hand, can act equally as H-bond donor or acceptor [59] and therefore they can locate close to both ester as well as head groups. Moreover, the presence of one additional oxygen atom in HO_2 compared to the OH radicals results in stronger van der Waals interactions with lipid head groups [59], which might explain

Table 1
Calculated free energy barriers of ROS across native and 50% (peroxide and aldehyde) oxidized PLBs. The values given for H_2O_2, HO_2 and OH are the activation free energies for permeation, i.e., to reach the bilayer center, whereas it is an activation free energy relative to the aqueous phase in the case of O_2 (cf. Fig. 3).

System	Activation free energy (kJ/mol)			
	H_2O_2	OH	HO_2	O_2
Native	34.5 ± 2.1	20.2 ± 2.1	21.3 ± 2.2	8.3 ± 1.1
50% peroxide	36.4 ± 3.4	18.6 ± 2.5	17.6 ± 2.6	6.5 ± 1.4
50% aldehyde	23.8 ± 1.7	11.1 ± 1.2	15.8 ± 1.7	7.5 ± 2.1

Table 2
Summary of the area per lipid, the bilayer thickness and the box size in the z-direction, in case of the native membrane as well as the 50% (peroxide and aldehyde) oxidized membranes.

System	Area per lipid (nm^2)	Bilayer thickness (nm)	L_z (nm)
Native	0.673 ± 0.001	3.89 ± 0.04	9.61 ± 0.02
50% peroxide	0.784 ± 0.002	3.24 ± 0.04	8.26 ± 0.03
50% aldehyde	0.809 ± 0.003	3.33 ± 0.06	8.08 ± 0.05

the deep free energy minimum shown for HO_2 (see Fig. 3). It should be mentioned here that H_2O_2 molecules are more stable in water solution, as they bind with water molecules at least with four hydrogen bonds, which was revealed in an ab initio MD study [72]. Moreover, H_2O_2 molecules establish about twice as many H-bonds in water as OH or HO_2 [59], which can explain why they cannot penetrate deeper in the membrane and they stay close to the aqueous phase and phosphate region (see Fig. 3). Nevertheless, all these hydrophilic ROS (i.e., H_2O_2, HO_2 and OH) experience permeation barriers by the membrane. This is consistent with experimental evidence, where HO_2 and H_2O_2 are found to be much less permeant than O_2 [73]. The calculated free energy barriers for all ROS are given in Table 1. It should be mentioned that the free energy barriers calculated using different force fields tend to be different (see e.g., parametric study of simple molecule partitioning applying various force fields in [74]). Therefore, we here pay specifically attention to the relative values, i.e., how lipid oxidation influences the overall free energy barriers of ROS (see Fig. 3 and Table 1), instead of to the absolute values.

The activation free energy for H_2O_2 permeation in the native PLB is 34.5 ± 2.1 kJ/mol, which is in reasonable agreement with the experimental value, i.e., 36.8 kJ/mol [75].

As is clear from Table 1, an overall decrease of the activation free energies of H_2O_2, HO_2 and OH for permeation is observed in the case of oxidized PLBs, especially for aldehyde oxidized PLBs. Moreover, it is clear from Fig. 3 that the free energy profiles of these species become narrower in the lipid center in the case of the oxidized PLBs. This indicates that in oxidized membranes the ROS are able to accumulate only around the head groups, except for the O_2 molecules (see Fig. 3bc). The decrease of the free energy barriers and the sharpening of the profiles can be explained below after careful analysis of the effect of oxidation on the PLBs.

Thorough analysis of the effect of oxidation on the structural and dynamic properties of the PLB showed that oxidation of the lipids leads to a higher disordering of the lipid tails, thereby increasing the lipid area and decreasing the bilayer thickness (see Table 2).

The larger area per lipid and the drop in bilayer thickness are due to the bending of the polar oxidized groups from the hydrophobic core towards the water interface, which is also described in literature [13,19]. Moreover, a recent simulation study showed that an addition of oxidized lipids to the system increases the water density in the head group region and shifts the density maximum of lipid atoms towards the bilayer center, thereby decreasing the membrane thickness [76]. Table 2 also illustrates that in case of the aldehyde oxidation product, the increase of the area per lipid is more pronounced than for the peroxide oxidation product, whereas the decrease of the bilayer thickness is smaller. This means that the total bilayer volume is larger in case of aldehyde oxidation, compared to peroxidation of the membrane. This can only be explained by the permeation of water molecules into the membrane (or in the head group region), which would make the bilayer swell. This phenomenon is illustrated in Fig. 4. The same conclusion can also be drawn by looking at the total size of the box along the z-axis (L_z). From Table 2, it is clear that L_z is smaller in the aldehyde oxidized system compared to its peroxidized counterpart, while the bilayer thickness is larger. This again can be explained by the permeation of water molecules into the lipid system, by which L_z decreases and the bilayer thickness increases.

Thus, in the case of aldehyde oxidation the increase in permeability of the PLB is more pronounced compared to the peroxidation case. This explains the overall decrease of the energy barriers of the ROS in the oxidized PLBs, especially in the aldehyde oxidation case (see Fig. 3 and Table 1). Note that in general the oxidation of lipids in the membrane changes the inside-the-bilayer conditions, and this in turn affects the free energy barriers, their heights as well as the positions of the minima (see Fig. 3), which strongly depend on the water dynamics around the model system [76]. It should also be mentioned that in both oxidation cases the ROS cannot remain stable at the center of the bilayer (as is the case in the native PLB; cf. the flat profiles and even small minima in the profiles in Fig. 3a), except for the O_2 molecules. This can again be explained by an increase in lipid disordering, which leads to an increase in fluidity of the PLB.

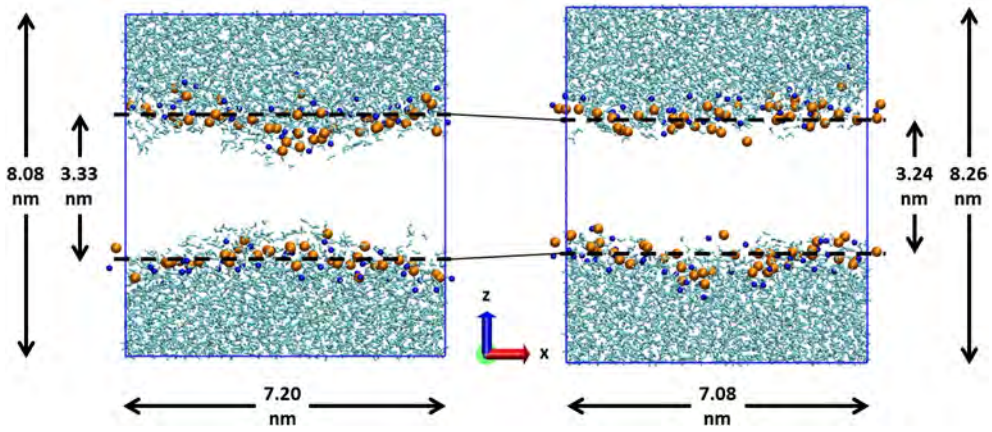

Fig. 4. Schematic illustration of the effect of oxidation on the bilayer thickness and on the box size along the z- and x-axis in case of the 50 mol% aldehyde oxidized system (left) and 50 mol% peroxidized system (right). Note that the box sizes along the x- and y-axis are identical ($L_x = L_y$). The lipid tails are not shown for the sake of clarity.

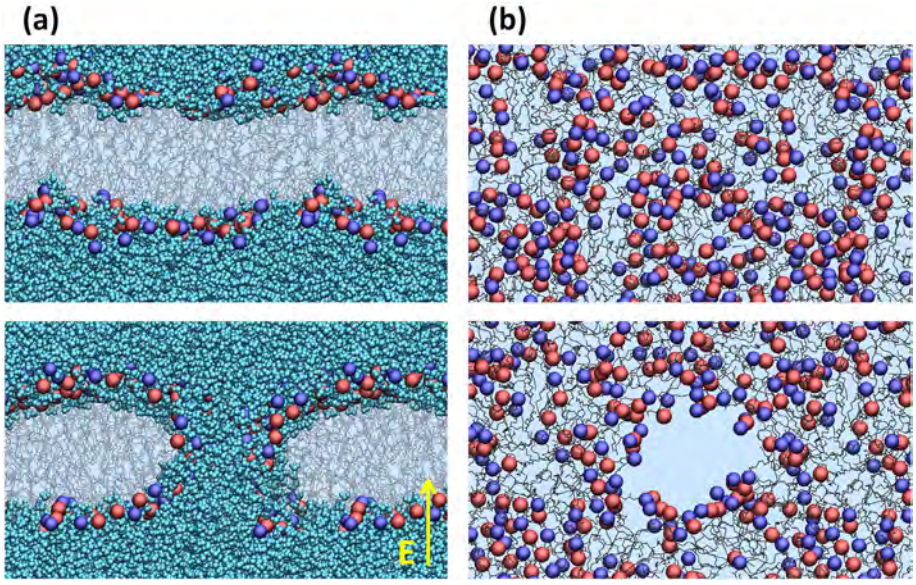

Fig. 5. Snapshots from MD simulations, showing the pore formation in a native PLB after ~2 ns, upon effect of a constant electric field of 0.5 V/nm, (a) side view and (b) top view. The water layers are removed from the top view picture, for the sake of clarity.

Generally we can conclude that oxidation of the lipid tails leads to a decrease of the lipid order, thereby increasing the bilayer fluidity as well as the permeability of the bilayer to ROS. However, the energy barriers still remain relatively high (order of tens of kJ/mol), so the ROS will not easily penetrate through the lipid bilayer. This indicates that specific protein channels, like AQPs, or pores are required in order to deliver the ROS into the cell interior.

3.2. Effect of the electric field on pore formation

As mentioned above, strong electric fields, i.e., in the range of 0.1–100 kV/cm, can lead to pore formation in the membrane. Some CAP sources produce quite strong electric fields, in addition to reactive plasma species, such as ROS, which cause lipid oxidation. Thus, it is important to know how oxidation of the lipids can affect the threshold electric field for poration, as well as the pore formation time. Fig. 5 demonstrates snapshots from MD simulations showing the typical pore formation process in a native PLB, under the effect of a constant electric field of 0.5 V/nm applied in the direction perpendicular to the bilayer surface. As mentioned above, the values of the electric field used in the MD simulations are not equivalent to the experimentally applied electric fields, and a detailed clarification of this comparison was given in Section 2.2 above. Therefore, the MD simulations are still very interesting to obtain information on the effect of electric fields on the electroporation process.

In short, the pore formation begins with the creation of a single-file water defect (i.e., a narrow aqueous channel with the width of a single water molecule), which grows quickly (within a few ns) eventually leading to the pore formation. This process is well described in literature (see e.g., [43,45]). This pore might allow ROS to penetrate into the cytoplasm, eventually to cause oxidative damage.

The average time needed to initiate pore formation in a native PLB is plotted as a function of the electric field value in Fig. 6. It is clear that a stronger electric field leads to a drop in the pore formation time. This behavior is more or less exponential, which is in agreement with [66].

It should be mentioned that the pore formation is a stochastic process, and therefore, the poration time can fluctuate considerably, as is obvious from the error bars in Fig. 6. Due to the stochastic nature of the process, there is an inherent uncertainty in the obtained values, which cannot be reduced by increasing the number of simulations.

Fig. 7 illustrates the average poration time for three different electric field values, as a function of the oxidation degree of the PLB, for both aldehyde (a) and peroxide (b) oxidation. It is clear from Fig. 7a that for aldehyde oxidation, a higher oxidation degree leads to a drop in the pore formation time. Moreover, electroporation can already occur upon applying lower electric fields compared to the native PLB (cf. Fig. 6 and the missing data points in Fig. 7a), which means that the lipid oxidation into aldehydes leads to a decrease of the threshold electric field needed for pore formation to occur. In the case of the peroxidation (see Fig. 7b), we did not observe the same strong effect of the oxidation on the pore formation time, although again a small drop is noticed compared to the native PLB.

The reason for this might be related to the permeability of water through the oxidized PLBs. Indeed, based on our results presented in Fig. 3, we may expect that the permeation free energy barrier of water through peroxidized PLBs will be higher than for aldehyde oxidation. Since the pore formation process initiates with the creation of water defects (see above), and since the penetration of water molecules to the hydrophobic part of the bilayer will be more difficult in the case of the

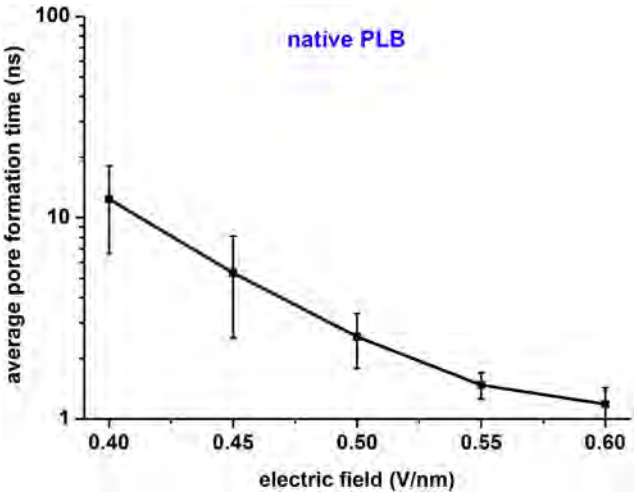

Fig. 6. Average time needed to initiate pore formation in a native PLB, versus the applied electric field.

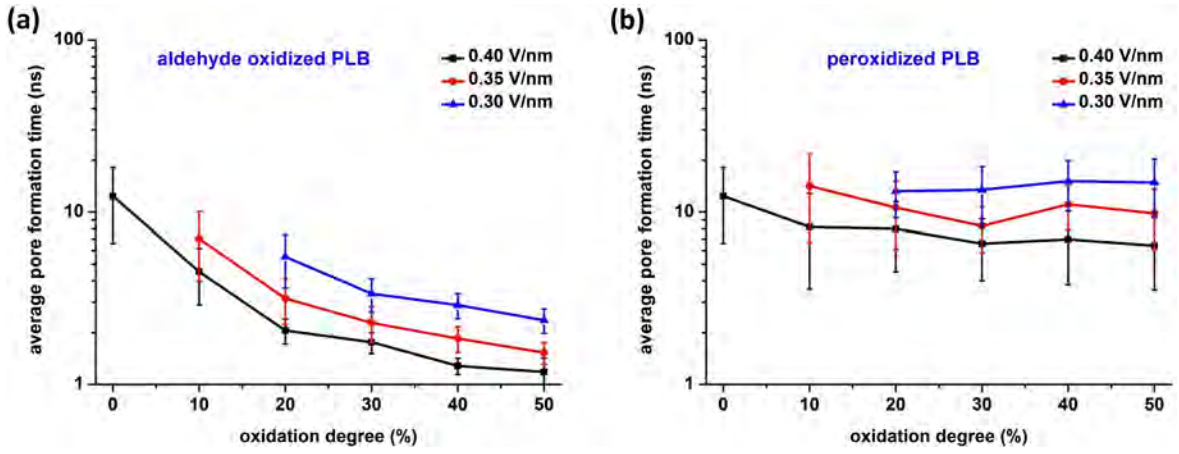

Fig. 7. Average time needed to initiate pore formation, for different applied electric fields, versus oxidation degree, for aldehyde oxidation (a) and peroxidation (b).

peroxidized PLB, more time will be needed for pore formation, independent from the oxidation degree (cf. Fig. 7).

We want to stress again that in electroporation simulations the applied electric fields are much higher than the fields used in experiments, which are typically in the order of few mV/nm [30,31]. As we mentioned above, these values should not be directly compared. For a more detailed clarification of this comparison, see Section 2.2 above. Moreover, the average pore formation times obtained in MD simulations (see Figs. 6 and 7) cannot be directly related to the experimentally observed pore formation kinetics, which is expressed by a characteristic time (τ), as they are conceptually different. Briefly, τ is an ensemble averaged value which is independent of the size of the PL patch, whereas in MD simulations with small PL structures, the probability of an occurrence of a first pore depends on the patch size (i.e., it increases with patch size). These issues were clarified in more detail in [77]. Thus, the attention should be paid on the trends and not on the exact values of the poration times and electric fields given in Figs. 6 and 7.

In general, we can conclude that oxidation of the lipid tails in the PLB facilitates the pore formation, by lowering the threshold electric field needed for pore formation.

4. Conclusions

In this study, computer simulations were performed to obtain a better insight in the synergistic effect of an electric field in combination with lipid oxidation on the formation of pores in a PLB. First, the translocation of ROS through native and oxidized PLBs was investigated in the absence of an electric field. It was found that oxidation of the PLs leads to an overall decrease of the permeation free energy barriers of the ROS, especially in the case of aldehyde oxidation. This is due to the increasing fluidity of the PLB, thereby increasing the permeability of the bilayer to ROS. However, the energy barriers are still relatively high, and thus the ROS will still not be able to easily travel through the oxidized PLB. This indicates that there is a need for specific protein channels, like AQPs, or that pores should be created in order to deliver reactive species into the cell interior.

The latter can be realized by applying an electric field, i.e., so-called electroporation. As some CAP sources produce significant electric fields, besides ROS which may lead to lipid oxidation, we investigated the synergistic effect of the electric field and oxidation of the PLB. Our calculations reveal that a stronger electric field yields a shorter pore formation time. Moreover, oxidation of lipid tails leads to a drop in the average time needed to initiate electroporation, as well as a lower threshold electric field needed for pore formation. This effect was most apparent for aldehyde oxidation, while it was rather minor for peroxidation of the PLB. The latter may be explained by the higher permeation free energy barrier of water through a peroxidized PLB, as the pore formation process is initiated by the creation of water defects.

The present results provide an atomic-level insight into the mechanisms of the combined effect of an electric field and lipid oxidation, as produced e.g., by cold atmospheric plasma, on living cells.

Transparency document

The Transparency document associated with this article can be found, in the online version.

Acknowledgements

This work is financially supported by the Fund for Scientific Research Flanders (FWO; grant numbers: 1200216N and 11U5416N). The work was carried out using the Turing HPC infrastructure of the CalcUA core facility of the Universiteit Antwerpen, a division of the Flemish Supercomputer Center VSC, funded by the Hercules Foundation, the Flemish Government (department EWI) and the Universiteit Antwerpen.

References

[1] M. Keidar, Plasma for cancer treatment, Plasma Sources Sci. Technol. 24 (2015) 033001.
[2] M. Keidar, R. Walk, A. Shashurin, P. Srinivasan, A. Sandler, S. Dasgupta, R. Ravi, R. Guerrero-Preston, B. Trink, Cold plasma selectivity and the possibility of a paradigm shift in cancer therapy, Br. J. Cancer 105 (2011) 1295–1301.
[3] X. Lu, G. Naidis, M. Laroussi, S. Reuter, D. Graves, K. Ostrikov, Reactive species in non-equilibrium atmospheric-pressure plasmas: generation, transport, and biological effects, Phys. Rep. 630 (2016) 1–84.
[4] E.A. Ratovitski, X. Cheng, D. Yan, J.H. Sherman, J. Canady, B. Trink, M. Keidar, Anti-cancer therapies of 21st century: novel approach to treat human cancers using cold atmospheric plasma, Plasma Process. Polym. 11 (2014) 1128–1137.
[5] J. Schlegel, J. Köritzer, V. Boxhammer, Plasma in cancer treatment, Clin. Plasma Med. 1 (2013) 2–7.
[6] D. Yan, A. Talbot, N. Nourmohammadi, J.H. Sherman, X. Cheng, M. Keidar, Toward understanding the selective anticancer capacity of cold atmospheric plasma—a model based on aquaporins (review), Biointerphases 10 (2015) 040801.
[7] S.J. Kim, H.M. Joh, T. Chung, Production of intracellular reactive oxygen species and change of cell viability induced by atmospheric pressure plasma in normal and cancer cells, Appl. Phys. Lett. 103 (2013) 153705.
[8] M. Ishaq, M.D. Evans, K.K. Ostrikov, Atmospheric pressure gas plasma-induced colorectal cancer cell death is mediated by Nox2–ASK1 apoptosis pathways and oxidative stress is mitigated by Srx–Nrf2 anti-oxidant system, Biochim. Biophysi. Acta Mol. Cell Res. 1843 (2014) 2827–2837.
[9] M. Ishaq, S. Kumar, H. Varinli, Z.J. Han, A.E. Rider, M.D. Evans, A.B. Murphy, K. Ostrikov, Atmospheric gas plasma–induced ROS production activates TNF-ASK1 pathway for the induction of melanoma cancer cell apoptosis, Mol. Biol. Cell 25 (2014) 1523–1531.
[10] N.K. Kaushik, N. Kaushik, D. Park, E.H. Choi, Altered antioxidant system stimulates dielectric barrier discharge plasma-induced cell death for solid tumor cell treatment, PLoS One 9 (2014), e103349. .

[11] S.J. Kim, T. Chung, Cold atmospheric plasma jet-generated RONS and their selective effects on normal and carcinoma cells, Sci. Rep. 6 (2016).
[12] E.J. Szili, S.-H. Hong, R.D. Short, On the effect of serum on the transport of reactive oxygen species across phospholipid membranes, Biointerphases 10 (2015) 029511.
[13] J. Van der Paal, E.C. Neyts, C.C. Verlackt, A. Bogaerts, Effect of lipid peroxidation on membrane permeability of cancer and normal cells subjected to oxidative stress, Chem. Sci. 7 (2016) 489–498.
[14] M.U. Hammer, E. Forbrig, S. Kupsch, K.-D. Weltmann, S. Reuter, IInfluence of plasma treatment on the structure and function of lipids, Plasma Med. 3 (2013).
[15] S. Maheux, G. Frache, J. Thomann, F. Clément, C. Penny, T. Belmonte, D. Duday, Small unilamellar liposomes as a membrane model for cell inactivation by cold atmospheric plasma treatment, J. Phys. D. Appl. Phys. 49 (2016) 344001.
[16] S.-H. Hong, E.J. Szili, A.T.A. Jenkins, R.D. Short, Ionized gas (plasma) delivery of reactive oxygen species (ROS) into artificial cells, J. Phys. D. Appl. Phys. 47 (2014) 362001.
[17] S. Ki, J. Park, C. Sung, C. Lee, H. Uhm, E. Choi, K. Baik, Artificial vesicles as an animal cell model for the study of biological application of non-thermal plasma, J. Phys. D. Appl. Phys. 49 (2016) 085401.
[18] R. Tero, Y. Suda, R. Kato, H. Tanoue, H. Takikawa, Plasma irradiation of artificial cell membrane system at solid–liquid interface, Appl. Phys. Express 7 (2014) 077001.
[19] J. Wong-Ekkabut, Z. Xu, W. Triampo, I.-M. Tang, D.P. Tieleman, L. Monticelli, Effect of lipid peroxidation on the properties of lipid bilayers: a molecular dynamics study, Biophys. J. 93 (2007) 4225–4236.
[20] L. Beranova, L. Cwiklik, P. Jurkiewicz, M. Hof, P. Jungwirth, Oxidation changes physical properties of phospholipid bilayers: fluorescence spectroscopy and molecular simulations, Langmuir 26 (2010) 6140–6144.
[21] L. Cwiklik, P. Jungwirth, Massive oxidation of phospholipid membranes leads to pore creation and bilayer disintegration, Chem. Phys. Lett. 486 (2010) 99–103.
[22] E. Robert, T. Darny, S. Dozias, S. Iseni, J.-M. Pouvesle, New insights on the propagation of pulsed atmospheric plasma streams: from single jet to multi jet arrays, Phys. Plasmas 22 (2015) 122007.
[23] A. Bourdon, T. Darny, F. Pechereau, J.-M. Pouvesle, P. Viegas, S. Iséni, E. Robert, Numerical and experimental study of the dynamics of a μs helium plasma gun discharge with various amounts of N2 admixture, Plasma Sources Sci. Technol. 25 (2016) 035002.
[24] A. Begum, M. Laroussi, M.R. Pervez, Atmospheric pressure He-air plasma jet: breakdown process and propagation phenomenon, AIP Adv. 3 (2013) 062117.
[25] G.B. Sretenović, I.B. Krstić, V.V. Kovačević, B.M. Obradović, M.M. Kuraica, Spatio-temporally resolved electric field measurements in helium plasma jet, J. Phys. D. Appl. Phys. 47 (2014) 102001.
[26] A. Shashurin, M. Shneider, M. Keidar, Measurements of streamer head potential and conductivity of streamer column in cold nonequilibrium atmospheric plasmas, Plasma Sources Sci. Technol. 21 (2012) 034006.
[27] N.Y. Babaeva, M.J. Kushner, Intracellular electric fields produced by dielectric barrier discharge treatment of skin, J. Phys. D. Appl. Phys. 43 (2010) 185206.
[28] N.Y. Babaeva, W. Tian, M.J. Kushner, The interaction between plasma filaments in dielectric barrier discharges and liquid covered wounds: electric fields delivered to model platelets and cells, J. Phys. D. Appl. Phys. 47 (2014) 235201.
[29] C. Douat, G. Busco, V. Vijayarangan, S. Dozias, S. Iséni, X. Damany, C. Grillon, A. Delalande, C. Pichon, M. Dezet, A.-L. Bulteau, J.-M. Pouvesle, E. Robert, Challenges in the transition from in vitro to in vivo experiments: source effects and biological aspects, IWPCT3, Washington, United States, 2016.
[30] A.M. Hirst, F.M. Frame, M. Arya, N.J. Maitland, D. O'Connell, Low temperature plasmas as emerging cancer therapeutics: the state of play and thoughts for the future, Tumor Biol. (2016) 1–11.
[31] J.C. Weaver, K.C. Smith, A.T. Esser, R.S. Son, T. Gowrishankar, A brief overview of electroporation pulse strength–duration space: a region where additional intracellular effects are expected, Bioelectrochemistry 87 (2012) 236–243.
[32] M.L. Yarmush, A. Golberg, G. Serša, T. Kotnik, D. Miklavčič, Electroporation-based technologies for medicine: principles, applications, and challenges, Annu. Rev. Biomed. Eng. 16 (2014) 295.
[33] S. Lakshmanan, G.K. Gupta, P. Avci, R. Chandran, M. Sadasivam, A.E.S. Jorge, M.R. Hamblin, Physical energy for drug delivery; poration, concentration and activation, Adv. Drug Deliv. Rev. 71 (2014) 98–114.
[34] S. Haberl, D. Miklavcic, G. Sersa, W. Frey, B. Rubinsky, Cell membrane electroporation–part 2: the applications, IEEE Electr. Insul. Mag. 29 (2013) 29–37.
[35] J. Villemejane, L.M. Mir, Physical methods of nucleic acid transfer: general concepts and applications, Br. J. Pharmacol. 157 (2009) 207–219.
[36] M. Breton, L.M. Mir, Microsecond and nanosecond electric pulses in cancer treatments, Bioelectromagnetics 33 (2012) 106–123.
[37] J. Gehl, Electroporation: theory and methods, perspectives for drug delivery, gene therapy and research, Acta Physiol. Scand. 177 (2003) 437–447.
[38] A. Gothelf, L.M. Mir, J. Gehl, Electrochemotherapy: results of cancer treatment using enhanced delivery of bleomycin by electroporation, Cancer Treat. Rev. 29 (2003) 371–387.
[39] S.J. Beebe, N.M. Sain, W. Ren, Induction of cell death mechanisms and apoptosis by nanosecond pulsed electric fields (nsPEFs), Cells 2 (2013) 136–162.
[40] C. Chen, S. Smye, M. Robinson, J. Evans, Membrane electroporation theories: a review, Med. Biol. Eng. Comput. 44 (2006) 5–14.
[41] M. Cemazar, Y. Tamzali, G. Sersa, N. Tozon, L. Mir, D. Miklavcic, R. Lowe, J. Teissie, Electrochemotherapy in veterinary oncology, J. Vet. Intern. Med. 22 (2008) 826–831.
[42] A.M. Bodles-Brakhop, R. Heller, R. Draghia-Akli, Electroporation for the delivery of DNA-based vaccines and immunotherapeutics: current clinical developments, Mol. Ther. 17 (2009) 585–592.
[43] D.P. Tieleman, The molecular basis of electroporation, BMC Biochem. 5 (2004) 1.
[44] P.T. Vernier, M.J. Ziegler, Nanosecond field alignment of head group and water dipoles in electroporating phospholipid bilayers, J. Phys. Chem. B 111 (2007) 12993–12996.
[45] M. Tarek, Membrane electroporation: a molecular dynamics simulation, Biophys. J. 88 (2005) 4045–4053.
[46] M. Casciola, D. Bonhenry, M. Liberti, F. Apollonio, M. Tarek, A molecular dynamic study of cholesterol rich lipid membranes: comparison of electroporation protocols, Bioelectrochemistry 100 (2014) 11–17.
[47] M. Breton, L. Delemotte, A. Silve, L.M. Mir, M. Tarek, Transport of siRNA through lipid membranes driven by nanosecond electric pulses: an experimental and computational study, J. Am. Chem. Soc. 134 (2012) 13938–13941.
[48] P.T. Vernier, M.J. Ziegler, Y. Sun, W.V. Chang, M.A. Gundersen, D.P. Tieleman, Nanopore formation and phosphatidylserine externalization in a phospholipid bilayer at high transmembrane potential, J. Am. Chem. Soc. 128 (2006) 6288–6289.
[49] A.Y. Antipina, A.A. Gurtovenko, Molecular mechanism of calcium-induced adsorption of DNA on zwitterionic phospholipid membranes, J. Phys. Chem. B 119 (2015) 6638–6645.
[50] M. Casciola, M. Tarek, A molecular insight into the electro-transfer of small molecules through electropores driven by electric fields, Biochim. Biophys. Acta Biomembr. 1858 (2016) 2278–2289.
[51] M. Tarek, Water and membranes: insights from molecular dynamics simulations, Water: The Forgotten Biological Molecule 2010, p. 139.
[52] S.J. Marrink, A.H. de Vries, D.P. Tieleman, Lipids on the move: simulations of membrane pores, domains, stalks and curves, Biochim. Biophys. Acta Biomembr. 1788 (2009) 149–168.
[53] T. He, D. Liu, H. Xu, Z. Liu, D. Xu, D. Li, Q. Li, M. Rong, M.G. Kong, A 'tissue model' to study the barrier effects of living tissues on the reactive species generated by surface air discharge, J. Phys. D Appl. Phys. 49 (2016) 205204.
[54] E.J. Szili, J.W. Bradley, R.D. Short, A 'tissue model' to study the plasma delivery of reactive oxygen species, J. Phys. D. Appl. Phys. 47 (2014) 152002.
[55] D.B. Graves, Reactive species from cold atmospheric plasma: implications for cancer therapy, Plasma Process. Polym. 11 (2014) 1120–1127.
[56] A. Reis, M. Domingues, F.M. Amado, A. Ferrer-Correia, P. Domingues, Separation of peroxidation products of diacyl-phosphatidylcholines by reversed-phase liquid chromatography–mass spectrometry, Biomed. Chromatogr. 19 (2005) 129–137.
[57] L. Martínez, R. Andrade, E.G. Birgin, J.M. Martínez, PACKMOL: a package for building initial configurations for molecular dynamics simulations, J. Comput. Chem. 30 (2009) 2157–2164.
[58] S.-W. Chiu, S.A. Pandit, H. Scott, E. Jakobsson, An improved united atom force field for simulation of mixed lipid bilayers, J. Phys. Chem. B 113 (2009) 2748–2763.
[59] R.M. Cordeiro, Reactive oxygen species at phospholipid bilayers: distribution, mobility and permeation, Biochim. Biophys. Acta Biomembr. 1838 (2014) 438–444.
[60] W.G. Hoover, Canonical dynamics: equilibrium phase-space distributions, Phys. Rev. A 31 (1985) 1695.
[61] M. Parrinello, A. Rahman, Polymorphic transitions in single crystals: a new molecular dynamics method, J. Appl. Phys. 52 (1981) 7182–7190.
[62] U. Essmann, L. Perera, M.L. Berkowitz, T. Darden, H. Lee, L.G. Pedersen, A smooth particle mesh Ewald method, J. Chem. Phys. 103 (1995) 8577–8593.
[63] M.J. Abraham, T. Murtola, R. Schulz, S. Páll, J.C. Smith, B. Hess, E. Lindahl, GROMACS: high performance molecular simulations through multi-level parallelism from laptops to supercomputers, SoftwareX 1 (2015) 19–25.
[64] S. Kumar, J.M. Rosenberg, D. Bouzida, R.H. Swendsen, P.A. Kollman, The weighted histogram analysis method for free-energy calculations on biomolecules. I. The method, J. Comput. Chem. 13 (1992) 1011–1021.
[65] P.T. Vernier, Z.A. Levine, Y.-H. Wu, V. Joubert, M.J. Ziegler, L.M. Mir, D.P. Tieleman, Electroporating fields target oxidatively damaged areas in the cell membrane, PLoS One 4 (2009), e7966. .
[66] A.A. Gurtovenko, A.S. Lyulina, Electroporation of asymmetric phospholipid membranes, J. Phys. Chem. B 118 (2014) 9909–9918.
[67] Q. Hu, S. Viswanadham, R. Joshi, K.H. Schoenbach, S.J. Beebe, P. Blackmore, Simulations of transient membrane behavior in cells subjected to a high-intensity ultrashort electric pulse, Phys. Rev. E 71 (2005) 031914.
[68] Q. Hu, R. Joshi, K. Schoenbach, Simulations of nanopore formation and phosphatidylserine externalization in lipid membranes subjected to a high-intensity, ultrashort electric pulse, Phys. Rev. E 72 (2005) 031902.
[69] L. Delemotte, M. Tarek, Molecular dynamics simulations of lipid membrane electroporation, J. Membr. Biol. 245 (2012) 531–543.
[70] B. Hess, Determining the shear viscosity of model liquids from molecular dynamics simulations, J. Chem. Phys. 116 (2002) 209–217.
[71] S.P. Chalmet, M.F. Ruiz-López, The structures of ozone and HOx radicals in aqueous solution from combined quantum/classical molecular dynamics simulations, J. Chem. Phys. 124 (2006) 194502.
[72] S.T. Moin, T.S. Hofer, B.R. Randolf, B.M. Rode, An ab initio quantum mechanical charge field molecular dynamics simulation of hydrogen peroxide in water, Comput. Theor. Chem. 980 (2012) 15–22.
[73] M.N. Möller, J.R. Lancaster, A. Denicola, The interaction of reactive oxygen and nitrogen species with membranes, Curr. Top. Membr. 61 (2008) 23–42.
[74] I. Vorobyov, W.D. Bennett, D.P. Tieleman, T.W. Allen, S. Noskov, The role of atomic polarization in the thermodynamics of chloroform partitioning to lipid bilayers, J. Chem. Theory Comput. 8 (2012) 618–628.

[75] J.C. Mathai, V. Sitaramam, Stretch sensitivity of transmembrane mobility of hydrogen peroxide through voids in the bilayer. Role of cardiolipin, J. Biol. Chem. 269 (1994) 17784–17793.
[76] G. Singh, A.C. Chamberlin, H.R. Zhekova, S.Y. Noskov, D.P. Tieleman, Two-dimensional potentials of mean force of Nile red in intact and damaged model bilayers. Application to calculations of fluorescence spectra, J. Chem. Theory Comput. 12 (2015) 364–371.
[77] R.A. Böckmann, B.L. De Groot, S. Kakorin, E. Neumann, H. Grubmüller, Kinetics, statistics, and energetics of lipid membrane electroporation studied by molecular dynamics simulations, Biophys. J. 95 (2008) 1837–1850.
[78] J. Van der Paal, C. Verheyen, E.C. Neyts, A. Bogaerts, Hampering effect of cholesterol on the permeation of reactive oxygen species through phospholipids bilayer: possible explanation for plasma cancer selectivity, Sci. Rep. 7 (2017) 39526.